Physics of Fluids

Experimental study of natural convection in a V-shape-section cavity

Cite as: Phys. Fluids **33**, 014104 (2021); https://doi.org/10.1063/5.0031104
Submitted: 29 September 2020 • Accepted: 16 December 2020 • Published Online: 08 January 2021

Xingyu Wang (王兴宇), **Sidhartha Bhowmick**, **Zhao Feng Tian** (田兆丰), **et al.**

Physics of Fluids ARTICLE scitation.org/journal/phf

Experimental study of natural convection in a V-shape-section cavity

Cite as: Phys. Fluids 33, 014104 (2021); doi: 10.1063/5.0031104
Submitted: 29 September 2020 • Accepted: 16 December 2020 •
Published Online: 8 January 2021

Xingyu Wang (王兴宇),[1] Sidhartha Bhowmick,[2] Zhao Feng Tian (田兆丰),[3] Suvash C. Saha,[4] and Feng Xu (徐丰)[1,a)]

AFFILIATIONS

[1]School of Civil Engineering, Beijing Jiaotong University, Beijing 100044, China
[2]Department of Mathematics, Jagannath University, Dhaka 1100, Bangladesh
[3]School of Mechanical Engineering, The University of Adelaide, Adelaide, SA 5005, Australia
[4]School of Mechanical and Mechatronic Engineering, University of Technology Sydney, Sydney, New South Wales 2007, Australia

[a)]**Author to whom correspondence should be addressed:** fxu@bjtu.edu.cn

ABSTRACT

Natural convection in a V-shaped section cavity heated from below and cooled from above is investigated experimentally for the first time in the literature. Temperature measurements using fast-response thermistors and flow visualization using the shadowgraph technology have been performed. The natural convection development in the cavity including the conductional, the transitional, and the fully developed stages is described. It is experimentally proven that the scaling law of the thermal boundary layer thickness is $\delta_T \sim (\kappa t)^{1/2}$ and the scaling law of the plume velocity is $v_p \sim \kappa Ra^{7/15}/l$. Furthermore, the occurrence of Hopf bifurcation in the transition to chaos and the flow structure are also identified experimentally. The power spectral density of the temperature time series reveals that the dominant frequency of the oscillations of the unsteady flow depends on the Rayleigh number, which is quantified.

NOMENCLATURE

A	aspect ratio
f	frequency (Hz)
f_p	peak frequency (Hz)
g	acceleration in gravity (m/s^2)
Gr	Grashof number
h, l, and w	height, length, and width of the cavity (m)
Nu	Nusselt number
Pr	Prandtl number
Ra	Rayleigh number
T	temperature (K)
T_0	initial temperature (K)
T_c	temperature of the cold top wall (K)
T_h	temperature of the hot inclined wall (K)
t	time (s)
v	velocity of puffing in the y-direction
v_p	velocity of the plume front in the y-direction
x, y, z	coordinates
β	coefficient of thermal expansion (1/K)
δ_T	thickness of the thermal boundary layer (m)
κ	thermal diffusivity (m^2/s)
ν	kinematic viscosity (m^2/s)
ρ	density (kg/m^3)

I. INTRODUCTION

Natural convection occurs widely in nature and industry such as in an attic, a reservoir, and a valley, where the boundaries are either horizontal or inclined. Accordingly, previous studies[1–5] have paid considerable attention to natural convection in these complex geometries, also involving that of horizontal and inclined heated plates.

It is well known that a thermal boundary layer forms in the fluid on a horizontal heated plate owing to heat transfer between the

fluid and the plate, as photographed by Stewartson[6] and Schmidt[7] and analyzed theoretically by Gill *et al.*[8] Additionally, the leading-edge effect (LEE) of the thermal boundary layer, the transition from one-dimensional flow to two-dimensional flow with oscillations, is found in the experiment for a semi-infinite heated plate studied by Rotem and Claassen.[9] The previous study by Rotem and Claassen[10] also shows that the leading-edge effect from the edges of the finite heated plate moves and meets at the center. The heated fluid at the center of the plate may further feed an upward plume, which is termed a starting plume by Turner.[11] Recently, the regimes of the lapping flows and the starting plume on the horizontal heated plate have also been analyzed and the scaling laws are obtained by Jiang *et al.*[12] The balance is between the buoyancy-induced horizontal pressure gradient term and the viscous term in the lapping flows. The buoyancy term balances the viscous term at the early time and then the inertial term in the starting plume. The transition time depends on the Rayleigh number.

Natural convection and heat transfer on an inclined heated plate are also interesting and thus investigated analytically and experimentally by Rich.[13] Temperature and velocity fields on an inclined plate are presented by Pera and Gebhart.[14] Furthermore, boundary-layer equations are used to analyze natural convection on an inclined heated plate by Kierkus[15] such that the theoretical results of the boundary-layer solution are also validated by the experiment. Additionally, the experiment shows that the flow may separate from the inclined heated plate with the increase in the Rayleigh number.[16] As the Rayleigh number is further increased, the flow could be unsteady or even turbulent.[17–19]

One important application of natural convection in inclined plates is found in the attic setup. The temperature of the roof of the attic varies significantly across daytime and nighttime, which usually induces complex flows in the attic. Flack conducted an experiment of natural convection in a cavity with a triangular cross section heated at the top boundaries (corresponding to the daytime situation) and found that the flow was always stable and laminar with two counter symmetric cells.[20] The transition from two cells to multiple cells is dependent on both the Rayleigh number and the aspect ratio (the height to base ratio).[21,22] In the case of cooling at the top (corresponding to the nighttime situation) and heating at the bottom, the transient flow in the cavity following start-up is described based on the numerical and experimental results in the work of Lei *et al.*[23] The three stages—an early, a transitional, and a steady or quasi-steady stage—are classified. For the steady stage, the flow in the cavity remains laminar and symmetrical for the Rayleigh number smaller than 4.39×10^6.[20] As the Rayleigh number is increased, a pitchfork bifurcation may occur; that is, an asymmetric flow appears in the cavity.[24] The critical Rayleigh number for the pitchfork bifurcation increases as the aspect ratio increases. The flow can also be chaotic if the Rayleigh number becomes larger than 6.18×10^6.[20] Furthermore, the three-dimensional structure with transversal and longitudinal rolls in the transition period is characterized.[21] The scaling law of the Nusselt number in the condition of cooling at the top wall but heating at the bottom wall, $Nu \sim A^{1/2}Pr^{1/4}Gr^{1/4}$, is also obtained using a scaling analysis by Poulikakos and Bejan,[25] where A is the aspect ratio, Pr is the Prandtl number, and Gr is the Grashof number.

Natural convection induced by daytime heating and nighttime cooling in near-shore waters plays an important part in water exchanges.[26] The study by Mao *et al.*[27] analyzes the dynamics of natural convection in a wedge-shaped section cavity and presents possible flow scenarios with different bottom slopes and maximum water depths. Furthermore, the study by Mao *et al.*[28] indicates that, for the relatively large slope case, there exist three possible regimes. That is, for small Rayleigh numbers (e.g., $Ra < A^{-6}$), natural convection flows are stable; for intermediate Rayleigh numbers ($A^{-6} < Ra < Ra_c{}^3$, $Ra_c \approx 657.5$), heat transfer is dominated at the near-shore region by conduction, but at the offshore region by convection; and for large Rayleigh numbers ($Ra > Ra_c{}^3$), heat transfer is dominated at the near-shore region by conduction and at the central region by steady convection, but at the offshore region by unsteady convection. Naghib *et al.*[2] showed that the onset of instability occurs closer to the tip of the wedge-shaped section cavity, as the Rayleigh number is increased. A detailed scaling analysis has been used to quantify natural convection flows in the case of nighttime cooling in the study by Lei and Patterson.[29] Three regimes including a conductive regime ($Ra < A^{-2} < A^4Ra_c{}^3$), a transitional regime ($A^{-2} < Ra < A^4Ra_c{}^3$), and a convective regime ($A^{-2} < A^4Ra_c{}^3 < Ra$) are quantified. In addition, transient natural convection flows in the wedge-shaped section cavity have been visualized using shadowgraphs by Lei and Patterson[30] in which the flow development has three stages; namely, the initial growth stage, the transitional stage, and the quasi-steady stage. Instabilities such as plumes originating from the inclined bottom boundary layer have been observed.[30] The phenomena and mechanisms of transient natural convection flows have also been characterized and analyzed based on two- and three-dimensional numerical results by Lei and Patterson.[31,32]

Recently, natural convection flows in a V-shaped section cavity have received increasing attention owing to the application to local climates in valleys and the fluid dynamics in rivers.[33–36] For example, the breakup of the stratification the fluid in a V-shaped section cavity has been investigated.[3,35,37] Furthermore, the symmetric and asymmetric flows in a cavity heated from the below are discussed based on the two-dimensional numerical results.[36] A set of bifurcations with different flow structures is described. Additionally, the heat transfer of laminar and turbulent flows in a cavity has also been quantified.[33,34] The results show that a V-shaped wall can increase heat transfer compared with a flat wall.

The literature review reveals that few studies have focused on the transition to chaos of natural convection flows in a V-shaped section cavity heated from the below other than the two dimensional numerical results by Bhowmick *et al.*[36] However, to the best knowledge of the authors, there is no experimental study on the transitional natural convection flow in a V-shaped section cavity in the literature. Only two experiments of natural convection in the similar geometry have been reported in the literature. One was carried out by Princevac and Fernando,[37] who considered the breakup of the stratification in a cold pool for small Rayleigh numbers, and the other was a study by Ruiz and Sparrow[33] considering heat transfer for the Rayleigh numbers ranging from 2×10^6 to 1.5×10^9 in a V-shaped corner. It is clear that since the top boundary condition is completely different, the flow structure and mechanisms of the natural convection flows in two similar geometries in this study are also different from those in this study for the medial Rayleigh numbers. Accordingly, a set of experiments here was performed for the Rayleigh number ranging from 1.29×10^5 to 1.29×10^6. The flow field in the unsteady steady stage and the bifurcation in

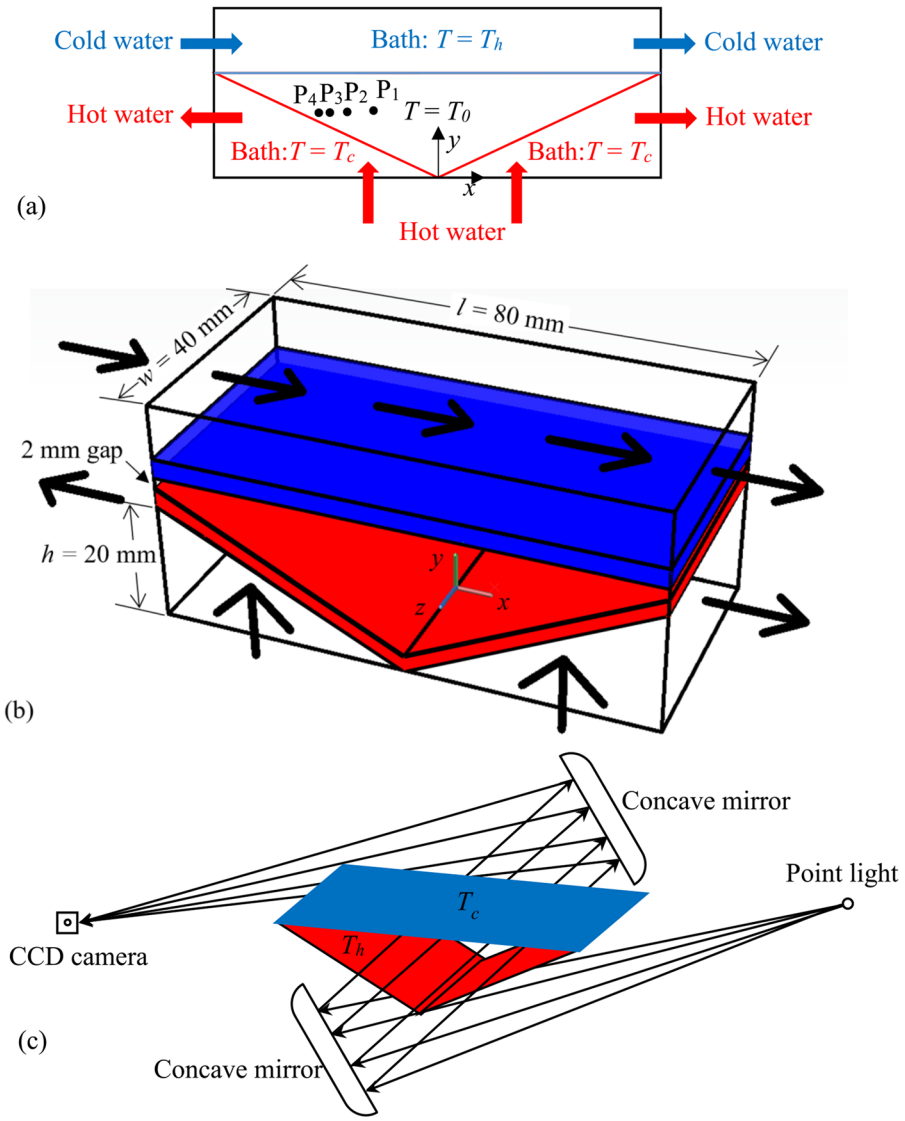

FIG. 1. Schematic of the experimental rig: (a) front view, (b) three-dimensional view (not to scale), and (c) shadowgraph setup. Four thermistors are mounted at different locations: P1 (−11.43 mm, 12.82 mm), P2 (−16.11 mm, 12.63 mm), P3 (−19.23 mm, 12.44 mm), and P4 (−21.22 mm, 12.37 mm), which are in the *xy* plane at $z = 0$ (the middle of the cavity in the *z* direction). Here, the origin of the coordinates is at the bottom corner.

the fully developed stage are analyzed based on the measurements. The shadowgraph is used to record flow images and thermistors are used to measure temperature time series at different locations in the cavity.

II. EXPERIMENTAL RIG AND MEASUREMENT

In this study, we performed a set of experiments for the natural convection in a V-shaped section cavity [with internal dimensions of 20 mm height, 80 mm length, and 40 mm width, as shown in Fig. 1(b)], heated from below and cooled from above, with water as the working fluid. A shadowgraph was used to visualize the flow structure, and thermistors were employed to record temperature time series in the cavity.

A. Experimental rig

The experimental rig is illustrated in Fig. 1(a). The V-shaped section cavity consists of a top wall, two inclined bottom walls, and front and back walls. Here, the top wall is a nickel-coated copper plate of 80 × 40 × 3 mm^3 for cooling the fluid in the cavity, and the two inclined walls are nickel-coated copper plates of 43 × 40 × 3 mm^3 for heating the fluid in the cavity; the front and back walls are made up of a 10 mm thick optical Perspex plate for flow visualization. Additionally, two small 2-mm-thick insulating rubber pads are inserted between the top and inclined copper plates at each edge for heat insulation between the top and bottom walls such that the cross section of the cavity is not completely triangular, as shown in Fig. 2(b). Such a variance does not have significant impact on the flow and heat transfer in the cavity.[36,38] The dimensions of the V-shaped section cavity are as follows: height $h = 20$ mm, width

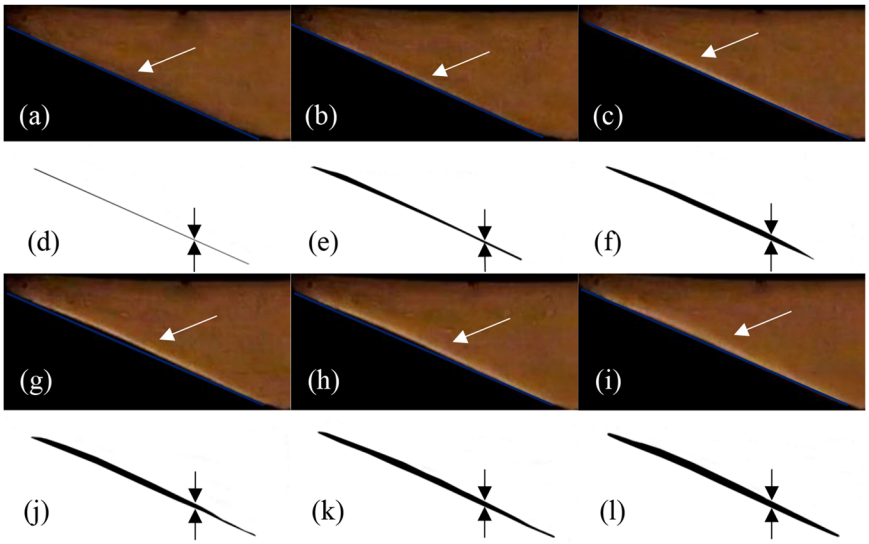

FIG. 2. Shadowgraph and processing images of the thermal boundary layer in the conductional stage for $Ra = 5.16 \times 10^5$. [(a) and (d)] $t = 1$ s, [(b) and (e)] $t = 3$ s, [(c) and (f)] $t = 5$ s, [(g) and (j)] $t = 7$ s, [(h) and (k)] $t = 9$ s, and [(i) and (l)] $t = 11$ s.

$w = 40$ mm, and length $l = 80$ mm. The bathes at the other side of the top or bottom wall [see Fig. 1(a)] were each connected to a circulator. One circulator supplies hot water to the bottom baths and the other one supplies cold water to the top bath. The hot and cold water flushing through the baths heats/cools the top and bottom walls to specified temperatures, T_c and T_h, respectively.

B. Measurement

The shadowgraph technology is used to visualize natural convection flows in the V-shaped section cavity, which has been widely employed in experimental studies of buoyancy-driven flows.[39–41] In the shadowgraph technique, initially, parallel light beams are usually set up, which pass through the observed fluid. The temperature of the fluid varies in space, which results in the variance in the refractive index of the fluid. Parallel light beams, after passing through the fluid, refract; as a result, a light pattern of varying intensity called a shadowgraph image is obtained (see Fig. 2). The study by Merzkirch[42] indicates that the light intensity in the shadowgraph image is very sensitive to the spatial derivative of the refractive index and in turn to the temperature. A time series of shadowgraph images can be used to describe the temporal evolution of the flow.[39,41,42]

To visualize the flow using a shadowgraph, a zig-zagged optical system is set up, as illustrated in Fig. 1(c), which is the same as that used in Wang *et al.*[39] The light source placed at the focal point of the first spherical mirror is a 12 W light bulb covered with an opaque box with a 1-mm diameter hole. The 0.3-m diameter concave mirror collimates the expanded light beam and results in parallel light beams passing through the V-shaped section cavity in the direction perpendicular to the front and back walls. The other identical concave mirror refocuses light beams to the Canon digital camera (EOS 5D, 1080 × 1920 pixels^2) at the focal point.[43] Here, a continuous shooting function of 25 images per second is adopted to record a time series of shadowgraph images of the transient flow (also see Fig. 2).

In the experiment, the temperature is measured using thermistors (NTC), which are mounted at different locations near the left bottom wall in the cavity, as illustrated in Fig. 1(a). Each thermistor is controlled by the data acquisition system using Kickstart software. The temperature signal is recorded six to seven times per second, which resolves the oscillations of natural convection flows in the cavity. The error of the temperature measurement is ±0.02 K. In this study, the temperature measurement is performed separately to obtain high-quality images without thermistors.

C. Procedure

Before the start of each experiment, the water in the V-shaped section cavity remains quiescent and isothermal at $T_0 = 293.15$ K. Once the experiment starts up, the hot and cold water are flushed from the bottom and top water baths, respectively. The top wall is cooled at T_c and the bottom wall is heated at T_h. Here, the initial temperature of the fluid may be given by

$$T_0 = \frac{T_c + T_h}{2}. \tag{1}$$

Such a sudden heating and cooling method is often used in the experiment in previous studies, e.g., the studies of Deardorff and Willis[44] and Xu *et al.*[45] The conductivity of Perspex is small, and thus, the heat loss through the front and back Perspex walls is negligible in the experiment.[41]

Transient natural convection in a cavity is determined by three dimensionless parameters: the Rayleigh number Ra, the Prandtl number Pr, and the aspect ratio A.[45] They are correspondingly defined as follows:

$$Ra = \frac{g\beta(T_h - T_c)h^3}{\nu\kappa}, \tag{2}$$

$$Pr = \frac{\nu}{\kappa}, \tag{3}$$

$$A = \frac{h}{l/2}, \tag{4}$$

where g is the gravitational acceleration, β is the coefficient of thermal expansion, ν is the kinematic viscosity, and κ is the thermal diffusivity.

III. FLOWS

In the experiment for flow visualization, the temperature difference between the top and the bottom walls of the cavity ranges from 1 K to 10 K by changing T_h and T_c, corresponding to Rayleigh numbers from 1.29×10^5 to 1.29×10^6, as shown in Table I. The Prandtl number and the aspect ratio are $Pr = 7.02$ and $A = 0.5$, respectively. The development of transient natural convection after sudden heating and cooling can be classified into three stages: a conductional stage, a transitional stage, and a fully developed stage.

A. Conductional stage

The fluid in the V-shaped section cavity as mentioned above is isothermal initially and quiescent. At the beginning of the experiment, instantaneous heating and cooling conditions are imposed on the bottom and top walls, respectively. As a result, heat is conducted into the fluid in the cavity from the bottom wall, and thus, a thermal boundary layer forms along the inclined bottom wall, as shown in Figs. 2(a) and 2(d). Since the convective flow in the thermal boundary layer is weak early on, the heat conducted from the inclined wall cannot be completely convected away, and in turn, the thermal boundary layer grows up, as shown by the bright strips (marked by white arrows) of shadowgraph images in Figs. 2(a)–2(c) and 2(g)–2(i). That is, the thickness of the thermal boundary layer increases with time. Here, only the thermal boundary layer in the left half of the cavity is shown in Fig. 2 because the flow is approximately symmetrical early on.

For a better view, the shadowgraph image was also processed. The bright strip describing the thermal boundary layer was extracted from the shadowgraph image, as illustrated in Figs. 2(d)–2(f) and 2(j)–2(l). Here, the image processing is that the background image recorded before the start-up of the experiment is subtracted from the experimental image. Furthermore, the reversed gray level of the processed image with a dark strip is shown in Figs. 2(j)–2(l) (also see Ref. 45 for details of image processing) in which the thermal boundary layer can be described by the black strip for greater clarity. Clearly, the thickness increases with time. Further examination of experimental results shows that the thickness increases until $t = 7$ s and then becomes an approximately constant value. That is, conduction dominates in a very short time and then convection becomes sufficiently large for which the heat conducted from the inclined wall can completely convect away, and thus, the thermal boundary layer does not grow up.

Studies by Xu *et al.*,[41] Cui *et al.*,[46] and Zhai *et al.*[47] show that, in the conduction stage, the growth of the thermal boundary layer is consistent with a scaling relationship,

$$\delta_T \sim (\kappa t)^{1/2}. \tag{5}$$

To validate the scaling law (5), the thickness of the thermal boundary layer in Fig. 2 was measured. Here, the thickness is defined as the thickness of the dark strip shown in Fig. 2, which is the same as that used by Wang *et al.* Note that the thickness along the wall is similar at different locations in the early stage.[30,45] Thus, the thickness of the dark strip at $x = -13.3$ mm was chosen. Figure 3 plots the measured thickness vs $(\kappa t)^{1/2}$. A linear relationship between the thickness and $(\kappa t)^{1/2}$ is clear. This means that the scaling relationship is able to quantify the growth of the thermal boundary layer along the inclined wall in the conductional stage. Additionally, it is worth noting that the thickness, when exceeds 2 mm, oscillates for $Ra = 5.16 \times 10^5$, as shown in Fig. 3(a). As described by Rotem and Claassen,[9] this phenomenon is a result of the leading edge effect (LEE); that is, the overshoot may occur owing to the perturbations originating from the leading edge. The transitional stage starts after the overshoot passes, which is similar to that for the vertical thermal boundary layer.[45] Furthermore, the thickness of the thermal boundary layer at the steady state has a scaling law of $\delta_{Ts} \sim h/Ra^{1/4}$, as shown in Fig. 3(b), which is the same as that adjacent to a vertical or horizontal thermal boundary.

TABLE I. Parameter ranges covered in the experiments.

Ra	T_h (K)	T_c (K)	T_0 (K)
1.29×10^5	293.65	292.65	293.15
2.58×10^5	294.15	292.15	293.15
3.87×10^5	294.65	291.65	293.15
5.16×10^5	295.15	291.15	293.15
6.45×10^5	295.65	290.65	293.15
7.74×10^5	296.15	290.15	293.15
9.03×10^5	296.65	289.65	293.15
1.03×10^6	297.15	289.15	293.15
1.16×10^6	297.65	288.65	293.15
1.29×10^6	298.15	288.15	293.15

B. Transitional stage

The development of transient natural convection in the transitional stage is characterized by the starting plume. Clearly, the cold fluid accumulates under the top wall and a downward starting plume forms near the center of the cavity with time, as shown in Fig. 4(a). Here, the front of the starting plume is marked by a horizontal white line. As the time is increased further, the front travels downward in Fig. 4(c) and finally reaches the bottom wall in Fig. 4(e). For greater clarity, the front of the starting plume is also extracted after image processing, as illustrated in Figs. 4(b), 4(d), and 4(f). It is clear that the starting plume is asymmetric; that is, the starting plume moves downward in the right half of the cavity but not along the middle

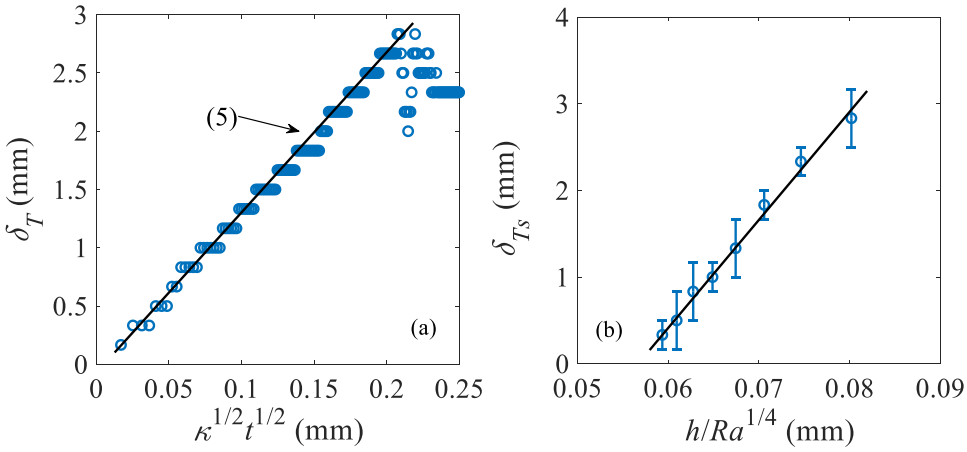

FIG. 3. (a) Thickness of the thermal boundary layer plotted against $\kappa^{1/2}t^{1/2}$ for $Ra = 5.16 \times 10^5$. (b) Thickness of the thermal boundary layer at steady state for different Rayleigh numbers, $\delta_{Ts} \sim h/Ra^{1/4}$.

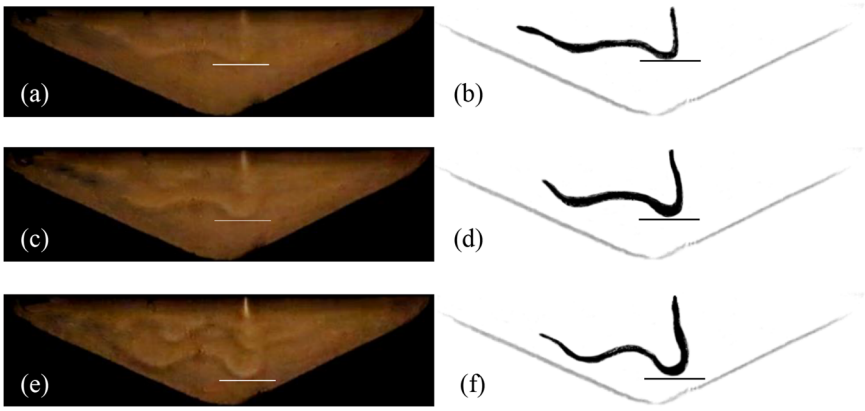

FIG. 4. Shadowgraph and processing images of a starting plume in the transitional stage for $Ra = 5.16 \times 10^5$. [(a) and (b)] t = 18 s, [(c) and (d)] t = 19 s, and [(e) and (f)] t = 20 s.

vertical line. Studies by Bhowmick *et al.*[36] and Cui *et al.*[38] show that such an asymmetric flow results from the Pitchfork bifurcation for large Rayleigh numbers where the flow could be on the right or the left, depending on the initial perturbations. In addition, the plume front is "W" shaped. This is a result of the instability of the plume front due to experimental perturbations.[48]

To describe the starting plume further, the relationship between the vertical coordinates of the plume front [shown by the black line

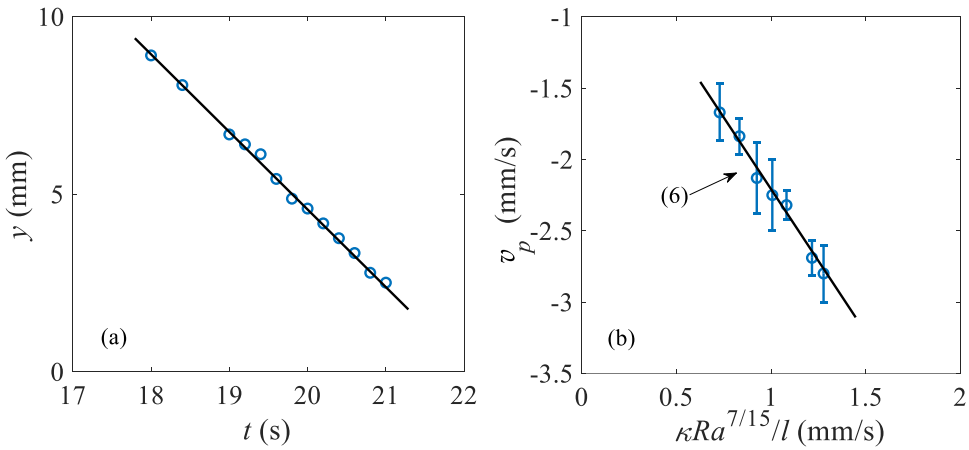

FIG. 5. (a) Vertical coordinate of the plume front at different times for $Ra = 5.16 \times 10^5$. (b) Dependence of the starting plume velocity on the Rayleigh number expression (6): $v_p \sim \kappa Ra^{7/15}/l$.

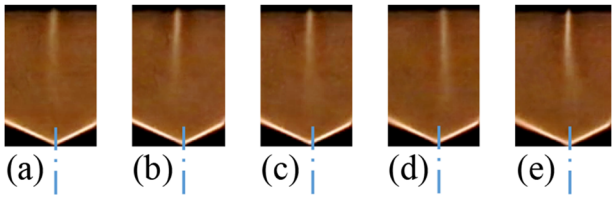

FIG. 6. Plume stem in the fully developed stage for $Ra = 5.16 \times 10^5$. (a) t = 1022 s, (b) t = 1041 s, (c) t = 1060 s, (d) t = 1079 s, and (e) t = 1098 s.

in Figs. 4(b), 4(d), and 4(f)] with time for $Ra = 5.16 \times 10^5$ is plotted in Fig. 5(a). The linear relationship between the vertical coordinate and time is obvious. This means that the front of the starting plume moves downwards at a constant velocity. The scaling analysis by Jiang *et al.*[12] indicates that the velocity under a balance of buoyancy and viscous force follows the scaling law,

$$v_p \sim \frac{\kappa Ra^{7/15}}{l}, \tag{6}$$

where v_p is the velocity of the plume front in the y direction. To validate the scaling law (6), the velocity of the front was calculated for $Ra = 5.16 \times 10^5$ based on the data shown in Fig. 5(a). The calculation was also performed for other Rayleigh numbers. Figure 5(b) shows the measured velocity and the scaling prediction for the different Rayleigh numbers. The approximately linear relationship between v_p and $\kappa Ra^{7/15}/l$ means that the scaling relationship (6) is able to describe the development of the starting plume in quantity.

C. Fully developed stage

As time increases, the transient natural convection develops further. Figure 6 shows the oscillations in the fully developed stage. It is clearly shown that the plume stem is oscillating around the vertical center line (marked by the white dashed line). In fact, this is the result of a Hopf bifurcation, as indicated by Bhowmick *et al.*[36] That is, the transition from the steady to unsteady state occurs as the Rayleigh number exceeds the critical value for the occurrence of a Hopf bifurcation.[49]

To quantify the plume stem further, the horizontal coordinate of the plume stem at a certain height was measured. Figure 7(a) shows the horizontal coordinate in the fully developed stage for

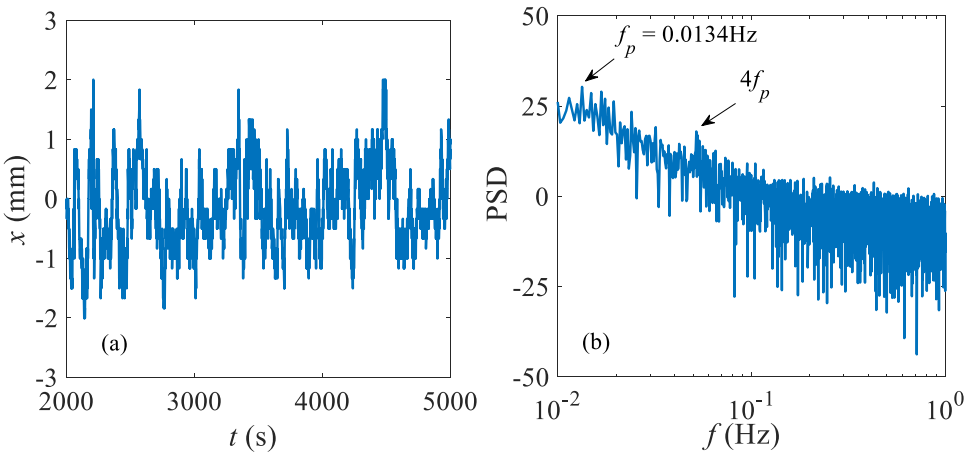

FIG. 7. Oscillations of the plume stem for $Ra = 5.16 \times 10^5$. (a) Horizontal coordinate of the plume stem at y = 180 mm. (b) Power spectral density (PSD).

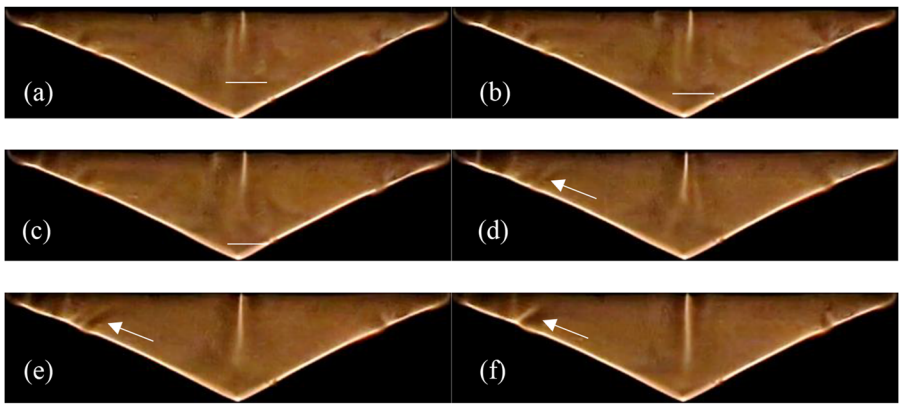

FIG. 8. Oscillations of plume for $Ra = 9.03 \times 10^5$. (a) t = 1772 s, (b) t = 1773 s, (c) t = 1774 s, (d) t = 1777 s, (e) t = 1779 s, and (f) t = 1781 s.

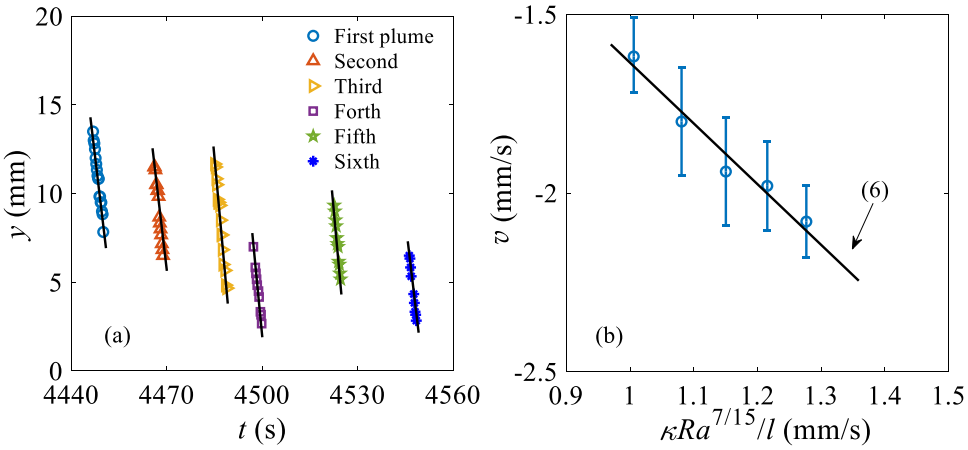

FIG. 9. (a) The y coordinate of the plume front for $Ra = 9.03 \times 10^5$. (b) Velocity of oscillations of the plume for different Rayleigh numbers (6): $v \sim \kappa Ra^{7/15}/l$.

$Ra = 5.16 \times 10^5$. The time series of x coordinates in Fig. 7(a) implies that the plume stem is oscillating around the center line over time. Furthermore, a spectral analysis was performed, and the power spectral density (PSD) is plotted in Fig. 7(b). Obviously, the dominant frequency of the oscillations is $f_p = 0.0134$ Hz, which is consistent with those shown in Fig. 6. In addition, the power spectral density reveals that there exists another frequency, $4f_p = 0.0528$ Hz, which is a harmonic frequency.[50]

As the Rayleigh number increases, the flow in the cavity becomes more chaotic. Figure 8 shows the evolutions of the plume emanating from the cooled top wall for $Ra = 9.03 \times 10^5$. When Ra is sufficiently large, the front of the plume is also clear in the fully developed stage, as illustrated by the short white line in Fig. 8(a). Then, the front descends and even reaches the bottom corner, as shown in Figs. 8(b) and 8(c). Furthermore, the front, as marked by the white arrow in Fig. 8(d), travels on an inclined wall after it reaches the bottom corner. As shown in Fig. 8(e), the front continues moving downstream and finally reaches the top corner, as shown in Fig. 8(f). That is, although the bulge due to instability in the lapping flow under the top wall[48] is not distinct here, there are similar instabilities in both the plume and the flow on the inclined wall, as shown in Figs. 8(d)–8(f).

To quantify the development of the plume in the fully developed stage, the position of the front in Fig. 8 was measured. Figure 9(a) shows the y coordinate of the oscillations of the plume front in which six successive plume fronts are presented. The linear relation between y and t is clear with an approximately constant velocity measured to be 1.73 (±0.2) mm/s. Furthermore, the velocity of the plume front is also plotted in Fig. 9(b). The scaling law of the velocity is consistent with that of the starting plume in the transitional stage in Fig. 5(b), i.e., $v \sim \kappa Ra^{7/15}/l$. However, the velocity value in Fig. 9(b) is lower than that of the stating plume shown in Fig. 5(b). This is because the temperature distribution is more uniform in the fully developed stage than at the start of the experiment, and in turn, the buoyancy force generated by the temperature gradient is smaller in the fully developed stage.

For further understanding of natural convection flows in the fully developed stage, Fig. 10 shows shadowgraph images for different Rayleigh numbers. Several studies[36,38] indicate that the flow is steady for small Rayleigh numbers, while Hopf bifurcation occurs with the increase in the Rayleigh number, under which the flow becomes unsteady and even may become chaotic if the Rayleigh number is sufficiently large. As illustrated by the arrowed lines in Fig. 10(a), which are plotted based on the observation of the experimental visualization, the flow is steady with two circulations for $Ra = 1.29 \times 10^5$. That is, the thermal boundary layers are on the inclined walls, while lapping flows are under the top wall moving to the center, and the downward plume is in the middle. For $Ra = 2.58 \times 10^5$, two small circulations appear in the corners, as marked in Fig. 10(b). When Ra is larger, for $Ra = 5.16 \times 10^5$, the

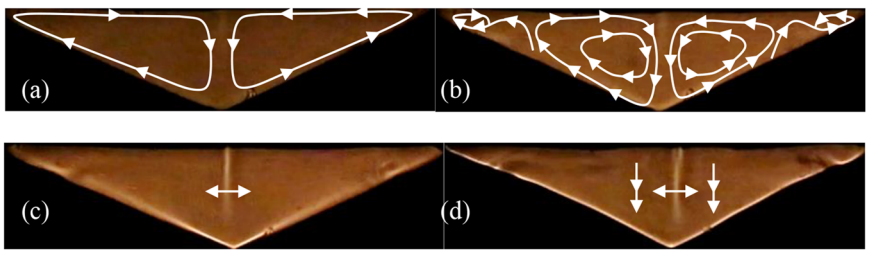

FIG. 10. Shadowgraph image in the fully developed stage for different Rayleigh numbers. (a) $Ra = 1.29 \times 10^5$, (b) $Ra = 2.58 \times 10^5$, (c) $Ra = 5.16 \times 10^5$, and (d) $Ra = 1.29 \times 10^6$.

oscillations appear and become distinct with the plume flapping at the middle, as marked by the arrow in Fig. 10(c) (also see Fig. 6). With the increase in the Rayleigh number, the oscillations become stronger with the plume flapping and oscillations at the middle, as illustrated in Fig. 10(d). That is, as the Rayleigh number increase, the thermal boundary layers and the plume stem become more obvious.

IV. TEMPERATURE TIME SERIES

To understand the flow oscillations in the cavity further, the temperature was also measured. Note that the location of the thermistor is illustrated in Fig. 1(a).

A. In the flow development for $Ra = 9.03 \times 10^5$

Figure 11(a) plots temperature time series measured at four locations. The oscillations are distinct from the start-up to the fully developed state, consistent with the flow visualization described before. It can be seen from this figure that the oscillations for thermistors 2, 3, and 4 are similar, with different amplitudes since they are located near the thermal boundary layer. When the oscillations travel downstream in the inclined thermal boundary layer, their amplitudes increase. The temperature of thermistor 1, which is located far from the thermal boundary layer, is also oscillatory but with lower amplitudes than those of the other three thermistors.

Figure 11(b) shows the first 150 s of the temperature time series plotted in Fig. 11(a). Clearly, the temperatures at all positions in the thermal boundary layer increase with time in the conductional stage. However, the temperature of thermistor 4 increases more rapidly owing to its location, which is closer to the heated wall. Additionally, the overshoot by LEE is also clear, as shown in Fig. 11(b).

Furthermore, the temperature decreases with the oscillations after the overshoot passes away and the development of natural convection enters the transitional stage. It is worth noting that the temperature of thermistor 1 decreases significantly. This is because thermistor 1 is inside the cavity, and thus, it is easy to measure the temperature of the fluid from the cold starting plume from the top wall (in addition, see Figs. 1 and 4).

For a better view, the temperature of thermistor 2 in the fully developed stage is also displayed in Fig. 11(c). Additionally, the spectral analysis has been carried out and the power spectral density

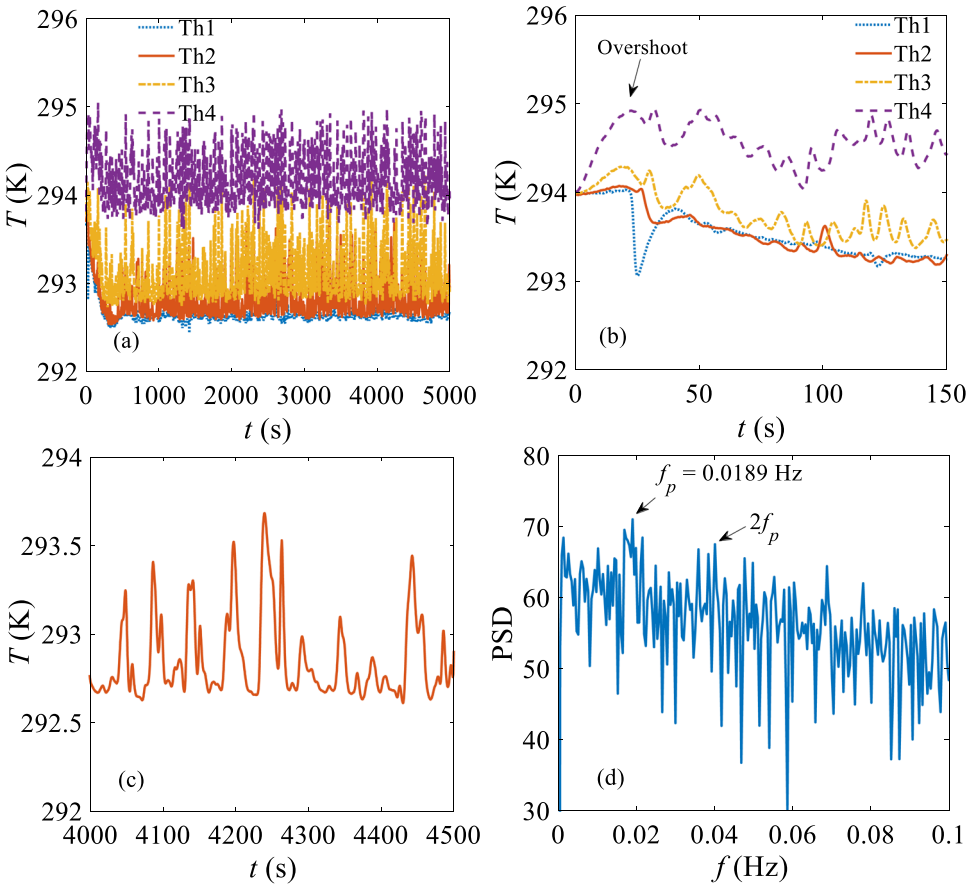

FIG. 11. Temperature and power spectral density of thermistors 1, 2, 3, and 4 for $Ra = 9.03 \times 10^5$. (a) Temperature from $t = 0$ to $t = 5000$ s. (b) Temperature from $t = 0$ to $t = 150$ s. (c) Temperature in the fully developed stage for thermistor 2. (d) PSD for thermistor 2.

is plotted in Fig. 11(d). It is clear that the dominant frequency is f_p = 0.0189 Hz with the harmonic mode.

B. In the fully developed stage for different Rayleigh numbers

Figure 12 shows the T2 temperature history from t = 2000 s to t = 5000 s for Rayleigh numbers $Ra = 1.29 \times 10^5$, $Ra = 3.87 \times 10^5$, $Ra = 5.16 \times 10^5$, and $Ra = 1.29 \times 10^6$ in the fully developed stage. It is clear that the average temperature becomes smaller with the increase in Rayleigh numbers because thermistor 2 is closed to the cooled wall even though the background temperature is fixed. Additionally, the temperature is oscillatory even for $Ra = 1.29 \times 10^5$, as shown in Fig. 12(a). As the Rayleigh number is increased, the oscillations become approximately periodic, as shown in the inset of Fig. 12(b), and more distinct, as shown in Fig. 12(c). Furthermore, for $Ra = 1.29 \times 10^6$, the amplitude of the oscillations become larger, but the flow may become more chaotic, as shown in Fig. 12(d).

The spectral analysis was also performed for temperature, as shown in Fig. 12. Figure 13 plots the power spectral density for different Rayleigh numbers. Clearly, the dominant frequency is f = 0.0015 Hz for $Ra = 1.29 \times 10^5$ in Fig. 13(a). However, as the Rayleigh number increases, the dominant frequency may change to f_p = 0.0126 Hz for $Ra = 3.87 \times 10^5$ in Fig. 13(b), f_p = 0.0129 Hz for $Ra = 5.16 \times 10^5$ in Fig. 13(c), and f_p = 0.0233 Hz for $Ra = 1.29 \times 10^6$ in Fig. 13(d) in which the harmonic mode is also clear. To understand the large variance of the frequency for different Rayleigh numbers, the temperature for the system of the circulator was measured. The examination of experimental results shows that the oscillations of the low frequency (0.0015 Hz) with very small amplitudes for small Rayleigh numbers in Fig. 13(a) (also see Fig. 12) originate from the system of the circulator for heating and cooling. The dominant frequency measured from temperature time series for $Ra = 5.16 \times 10^5$ is consistent with that from flow visualization shown in Fig. 7(b). In fact, as the Rayleigh number is increased, the appearance of the oscillations with the high frequency of f_p = 0.0126 Hz for $Ra = 3.87 \times 10^5$ is a result of Hopf bifurcation.[36] The further examination of experimental results shows that these dominant frequencies measured from the temperature time series for different Rayleigh numbers are also consistent with those from flow visualization in Sec. III.

Figures 13(c) and 13(d) show that the dominant frequency increases from f = 0.0126 Hz with $Ra = 3.87 \times 10^5$ to f = 0.0233 Hz with $Ra = 1.29 \times 10^6$. To quantify the relationship between the dominant frequency and the Rayleigh number, Fig. 14 shows the dominant frequency for various Rayleigh numbers. Here, the dominant frequency is normalized using $\kappa Ra^{1/2}/h^2$, which is the inverse of the time scale of the buoyancy-driven convective flow.[36,51] Clearly, $fh^2/(\kappa/Ra^{1/2})$ is ~0.0526 for $Ra \geq 5.16 \times 10^5$. This means that the relationship between the dominant frequency and $Ra^{1/2}$ is approximately linear for $Ra \geq 5.16 \times 10^5$ in the current experimental results.

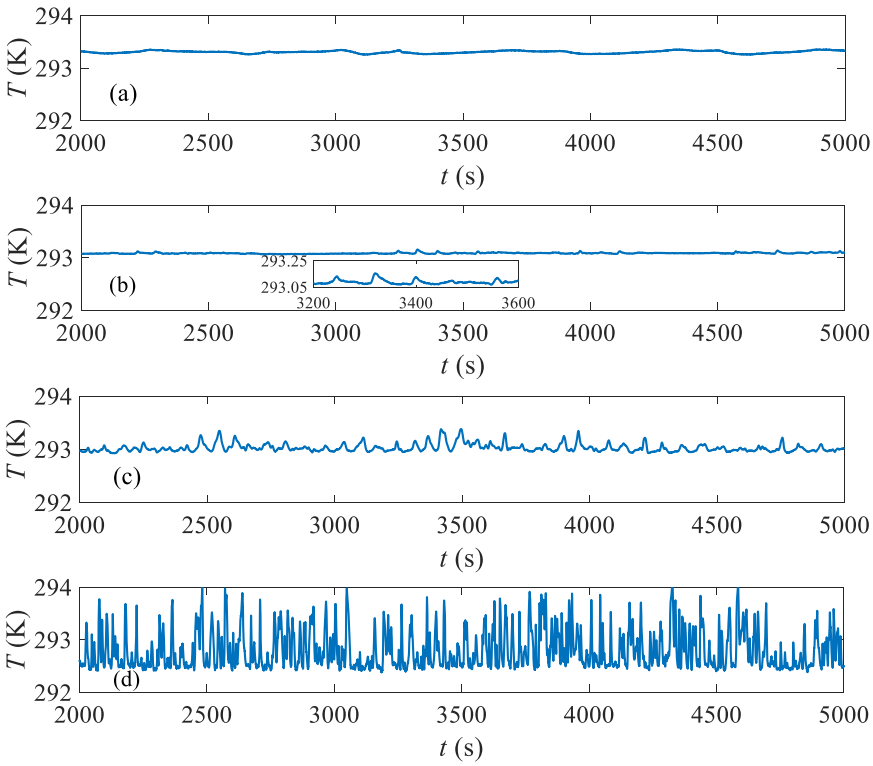

FIG. 12. Temperature time series for thermistor 2 for different Rayleigh numbers. (a) $Ra = 1.29 \times 10^5$, (b) $Ra = 3.87 \times 10^5$, (c) $Ra = 5.16 \times 10^5$, and (d) $Ra = 1.29 \times 10^6$.

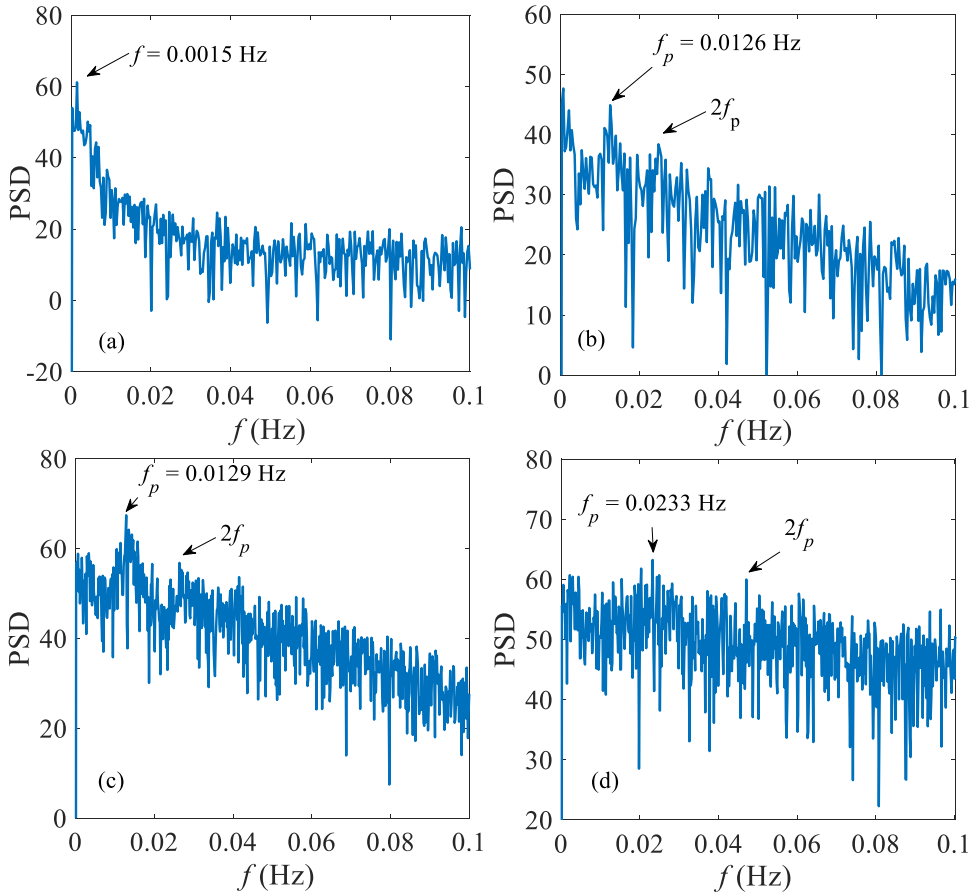

FIG. 13. Power spectral density of temperature time series for different Rayleigh numbers in Fig. 12. (a) $Ra = 1.29 \times 10^5$, (b) $Ra = 3.87 \times 10^5$, (c) $Ra = 5.16 \times 10^5$, and (d) $Ra = 1.29 \times 10^6$.

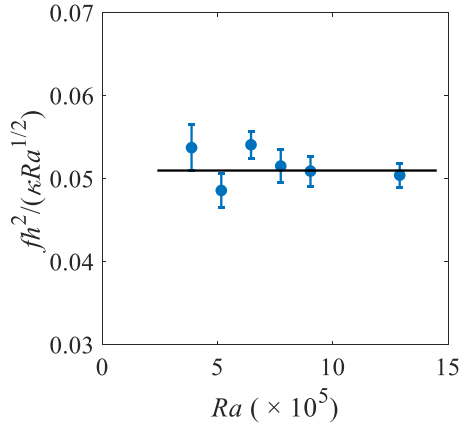

FIG. 14. Frequency of the temperature time series for different Rayleigh numbers.

V. CONCLUSIONS

Natural convection in the V-shaped section cavity, heated from below and cooled from above, was investigated experimentally. The Rayleigh numbers from 1.29×10^5 to 1.29×10^6 are considered in the experiment where $A = 0.5$ and $Pr = 7.02$. The development of transient natural convection after the start-up is characterized and described as the conductional, transitional, and fully developed stages.

The flow visualization reveals that the natural convection flow is weak in the conductional stage. The boundary layer is formed on the inclined wall and under the top wall after suddenly heating with the scaling of $(\kappa t)^{1/2}$. With the increase in time, the flow may become stronger and convection thus dominates heat transfer. The flow can be described by the starting plume from the top wall. The velocities of both the starting plume and the thermal boundary layer have been measured and are consistent with the scaling law of $v_p \sim \kappa Ra^{7/15}/l$.[12] The oscillation in the fully developed stage is characterized for various Rayleigh numbers. Additionally, the circulation is also described for various Rayleigh numbers.

Temperature time series by thermistors at different locations clearly characterize the growth of the thermal boundary layer in the conductional stage along with the starting plume and the oscillations in the transitional and fully developed stages. The oscillations in the fully developed stage are analyzed to demonstrate that the occurrence of Hopf bifurcation is proved and the dominant frequency is obtained from flow visualization and temperature measurement, respectively, which are consistent with each other. Furthermore,

the relationship between the dominant frequency and the Rayleigh number is quantified.

ACKNOWLEDGMENTS

This study was supported financially by the National Natural Science Foundation of China (Grant No. 11972072) and the 111 Project (Grant No. B13002). Additionally, the authors acknowledge Mrs. Alison-Jane Hunter at the University of Adelaide for proofreading the manuscript.

DATA AVAILABILITY

The data that support the findings of this study are available from the corresponding author upon reasonable request.

REFERENCES

[1]S. G. Perry and W. H. Snyder, "Laboratory simulations of the atmospheric mixed-layer in flow over complex topography," Phys. Fluids **29**(2), 020702 (2017).
[2]A. Naghib, J. Patterson, and C. Lei, "Natural convection induced by absorption of solar radiation in the near shore region of lakes and reservoirs: Experimental results," Exp. Therm. Fluid Sci. **90**, 101–114 (2018).
[3]K. Steenhauer, T. Tokyay, and G. Constantinescu, "Dynamics and structure of planar gravity currents propagating down an inclined surface," Phys. Fluids **29**(3), 036604 (2017).
[4]Y. Deng, C. He, P. Wang, and Y. Liu, "Unsteady behaviors of separated flow over a finite blunt plate at different inclination angles," Phys. Fluids **32**, 035111 (2020).
[5]F. Xu, S. Zhong, and S. Zhang, "Vortical structures and development of laminar flow over convergent-divergent riblets," Phys. Fluids **30**(5), 051901 (2018).
[6]K. Stewartson, "On the free convection from a horizontal plate," Z. Angew. Math. Phys. **9**, 276–282 (1958).
[7]E. Schmidt, "Schlierenaufnahmen des temperaturfeldes in der nähe wärmeabgebender körper," Forsch. Ing.-Wes. **3**, 181–189 (1932).
[8]W. N. Gill, D. W. Zeh, and E. Del-Casal, "Free convection on a horizontal plate," Z. Angew. Math. Phys. **16**, 539–541 (1965).
[9]Z. Rotem and L. Claassen, "Natural convection above unconfined horizontal surfaces," J. Fluid Mech. **39**, 173–192 (1969).
[10]Z. Rotem and L. Claassen, "Free convection boundary-layer flow over horizontal plates and discs," Can. J. Chem. Eng. **47**, 461–468 (1969).
[11]J. S. Turner, "Buoyant plumes and thermals," Annu. Rev. Fluid Mech. **1**, 29–44 (1969).
[12]Y. Jiang, B. Nie, and F. Xu, "Scaling laws of buoyant flows on a suddenly heated horizontal plate," Int. Commun. Heat Mass Transfer **105**, 58–64 (2019).
[13]B. R. Rich, "An investigation of heat transfer from an inclined flat plate in free convection," Trans. ASME **75**, 489–499 (1953).
[14]L. Pera and B. Gebhart, "Natural convection boundary layer flow over horizontal and slightly inclined surfaces," Int. J. Heat Mass Transfer **16**, 1131–1146 (1973).
[15]W. T. Kierkus, "An analysis of laminar free convection flow and heat transfer about an inclined isothermal plate," Int. J. Heat Mass Transfer **11**, 241–253 (1968).
[16]K. Komori, S. Kito, T. Nakamura, Y. Inaguma, and T. Inagaki, "Fluid flow and heat transfer in the transition process of natural convection over an inclined plate," Trans. ASME J. Heat Transfer **30**, 648–659 (2001).
[17]G. C. Vliet, "Natural convection local heat transfer on constant-heat-flux inclined surfaces," J. Heat Transfer **91**, 511–516 (1969).
[18]T. Fujii and H. Imura, "Natural-convection heat transfer from a plate with arbitrary inclination," Int. J. Heat Mass Transfer **15**, 755–767 (1972).
[19]H. Shaukatullah and B. Gebhart, "An experimental investigation of natural convection flow on an inclined surface," Int. J. Heat Mass Tranfer **21**, 1481–1490 (1978).
[20]R. D. Flack, "The experimental measurement of natural convection heat transfer in triangular enclosures heated or cooled from below," J. Heat Transfer **102**, 770–772 (1980).
[21]Y. E. Karyakin, Y. A. Sokovishin, and O. G. Martynenko, "Transient natural convection in triangular enclosures," Int. J. Heat Mass Transfer **31**, 1759–1766 (1988).
[22]H. Asan and L. Namli, "Laminar natural convection in a pitched roof of triangular cross-section: Summer day boundary conditions," Energy Build. **33**, 69–73 (2000).
[23]C. Lei, S. W. Armfield, and J. C. Patterson, "Unsteady natural convection in a water-filled isosceles triangular enclosure heated from below," Int. J. Heat Mass Transfer **51**, 2637–2650 (2008).
[24]G. A. Holtzman, R. W. Hill, and K. S. Ball, "Laminar natural convection in isosceles triangular enclosures heated from below and symmetrically cooled from above," J. Heat Transfer **122**, 485–491 (2000).
[25]D. Poulikakos and A. Bejan, "The fluid dynamics of an attic space," J. Fluid Mech. **131**, 251–269 (1983).
[26]Y. Mao, "Nearshore natural convection induced by a periodic thermal forcing at the water surface," Phys. Fluids **31**, 086604 (2019).
[27]Y. Mao, C. Lei, and J. C. Patterson, "Unsteady natural convection in a triangular enclosure induced by absorption of radiation: A revisit by improved scaling analysis," J. Fluid Mech. **622**, 75–102 (2009).
[28]Y. Mao, C. Lei, and J. C. Patterson, "Unsteady near-shore natural convection induced by surface cooling," J. Fluid Mech. **642**, 213–233 (2010).
[29]C. Lei and J. C. Patterson, "Unsteady natural convection in a triangular enclosure induced by surface cooling," Int. J. Heat Fluid Flow **26**, 307–321 (2005).
[30]C. Lei and J. C. Patterson, "Natural convection in a reservoir sidearm subject to solar radiation: Experimental observations," Exp. Fluids **32**(5), 590–599 (2002).
[31]C. Lei and J. C. Patterson, "Natural convection in a reservoir sidearm subject to solar radiation: A two-dimensional simulation," Numer. Heat Transfer **42**, 13–32 (2002).
[32]C. Lei and J. C. Patterson, "A direct three-dimensional simulation of radiation-induced natural convection in a shallow wedge," Int. J. Heat Mass Transfer **46**, 1183–1197 (2003).
[33]R. Ruiz and E. M. Sparrow, "Natural convection in V-shaped and L-shaped corners," Int. J. Heat Mass Transfer **30**, 2539–2548 (1987).
[34]S. Kenjereš, "Heat transfer enhancement induced by wall inclination in turbulent thermal convection," Phys. Rev. E **92**, 053006 (2015).
[35]S. Bhowmick, F. Xu, X. Zhang, and S. C. Saha, "Natural convection and heat transfer in a valley shaped cavity filled with initially stratified water," Int. J. Therm. Sci. **128**, 59–69 (2018).
[36]S. Bhowmick, S. C. Saha, M. Qiao, and F. Xu, "Transition to a chaotic flow in a V-shaped triangular cavity heated from below," Int. J. Heat Mass Transfer **128**, 76–86 (2019).
[37]M. Princevac and H. J. S. Fernando, "Morning breakup of cold pools in complex terrain," J. Fluid Mech. **616**, 99–109 (2008).
[38]H. Cui, F. Xu, and S. C. Saha, "A three-dimensional simulation of transient natural convection in a triangular cavity," Int. J. Heat Mass Transfer **85**, 1012–1022 (2015).
[39]X. Wang, F. Xu, and H. Zhai, "An experimental study of a starting plume on a mountain," Int. Commun. Heat Mass Transfer **97**, 1–8 (2018).
[40]D. J. Shlien, "Transition of the axisymmetric starting plume cap," Phys. Fluids **21**, 2154–2158 (1978).
[41]F. Xu, J. C. Patterson, and C. Lei, "An experimental study of the unsteady thermal flow around a thin fin on a sidewall of a differentially heated cavity," Int. J. Heat Fluid Flow **29**, 1139–1153 (2008).
[42]W. Merzkirch, *Flow Visualization* (Academic Press, New York, 1974).
[43]A. H. Zitouni, A. Arabi, Y. Salhi, Y. Zenati, E. K. Si-Ahmed, and J. Legrand, "Slug length and frequency upstream a sudden expansion in gas–liquid intermittent flow," Exp. Comput. Multiphase Flow **3**, 124–130 (2020).

[44]J. W. Deardorff and G. E. Willis, "Turbulence within a baroclinic laboratory mixed layer above a sloping surface," J. Atmos. Sci. **44**, 772–778 (1987).
[45]F. Xu, J. C. Patterson, and C. Lei, "Shadowgraph observations of the transition of the thermal boundary layer in a side-heated cavity," Exp. Fluids **38**, 770–779 (2005).
[46]H. Cui, F. Xu, and S. C. Saha, "Transition to unsteady natural convection flow in a prismatic enclosure of triangular section," Int. J. Therm. Sci. **111**, 330–339 (2017).
[47]H. Zhai, F. Xu, S. C. Saha, and Y. Hou, "Natural convection and heat transfer on a section-triangular roof," Int. Commun. Heat Fluid Flow **92**, 23–30 (2018).
[48]T. Hattori, N. Bartos, S. E. Norris, M. P. Kirkpatrick, and S. W. Armfield, "Experimental and numerical investigation of unsteady behaviour in the near-field of pure thermal planar plumes," Exp. Therm. Fluid Sci. **46**(46), 139–150 (2013).
[49]M. Qiao, Z. F. Tian, B. Nie, and F. Xu, "The route to chaos for plumes from a top-open cylinder heated from underneath," Phys. Fluids **30**, 124102 (2018).
[50]M. Qiao, Z. F. Tian, Q. Yang, and F. Xu, "Transition to chaos for buoyant flows in a groove heated from below," Phys. Fluids **32**, 054104 (2020).
[51]J. Patterson and J. Imberger, "Unsteady natural convection in a rectangular cavity," J. Fluid Mech. **100**, 65–86 (1980).